Facies analysis and diagenetic evolution of the Dinantian carbonates in the Dutch subsurface: data and analyses well BHG-01

Report by SCAN

October 2019

Ministerie van Economische Zaken en Klimaat
ebn
TNO
Interreg North-West Europe DGE-ROLLOUT

Facies analysis and diagenetic evolution of the Dinantian carbonates in the Dutch subsurface: data and analyses well BHG-01

Written by:
Mahtab Mozafari[1], Peter Gutteridge[2], Alberto Riva[3], Kees Geel[4], Joanna Garland[2] and Julie Dewit[2]

October 2019

1- Energie Beheer Nederland (EBN), Daalsesingel 1, 3511 SV Utrecht, the Netherlands
2- Cambridge Carbonates Ltd, No. 4 The Courtyard, 707 Warwick Road, Solihull, B91 3DA, UK
3- G.E.Plan Consulting srl, Via L. Ariosto 58, 44121 Ferrara, Italy
4- Geological Survey of the Netherlands (TNO), Princetonlaan 6, 3584 CB Utrecht, the Netherlands

Dit rapport is een product van het SCAN-programma en wordt mogelijk gemaakt door het Ministerie van Economische Zaken en Klimaat

Table of contents

1. Brouwershavense Gat-1 (BHG-01)

1.1 Introduction

The Brouwershavense Gat-1 (BHG-01) well was drilled in 1978, in the coastal area of Zeeland (Figure 1-1). It reached 2906 m TD in the Devonian Bollen Claystone. The well was a hydrocarbon exploration well but proved to be dry.

Figure 1-1: Map showing all the wells penetrating the Dinantian carbonates. Location of the BHG-01 well is indicated by dashed red circle.

Table 1-1: Table summarising the coordinates of the BHG-01 well (from www.nlog.nl).

Co-ordinates (x, y in utm31, ed50 format)	553226 / 5738089
Lat/Long (°)	51.79005597, 3.77168392
Supplied co-ordinates	43455 / 423528 RD
Depth in meters referred to:	Rotary Table
Total depth (m, along hole):	2906.8
Vertical position of Rotary Table:	23.58
Trajectory shape:	Deviated
Deviation in X-direction:	686.72
Deviation in Y-direction:	165.77
True vertical depth (TVD) in m:	2765.23

1.2 Available dataset

Most of the available data and reports on the BHG-01 well are available on "www.nlog.nl" within the following link:

https://www.nlog.nl/nlog/requestData/nlogp/allBor/metaData.jsp?tableName=BorLocation&id=106504916

The most relevant publications discussing and presenting the data obtained from BHG-01 well are as following:

Bless, M. J. M. (1978). Het Paleozoicum van de Diepboring Brouwershavensegat-1 (N.A.M.) tussen 1398 en 2906,8 m (5 bijlagen). Heerlen, Geologisch Bureau, 30 pp.

Buiskool Toxopeus, J. M. A., and Idiz, E. F. (1990). Geochemical investigation of two source rock extracts from well Brouwershavensche Gat-1, The Netherlands. Shell Research BV, Rijswijk, the Netherlands, 27 pp.

Buiskool Toxopeus, J. M. A., and Lieshout, J. B. van (1979). Maceral analysis of sediments penetrated by well Brouwershavensche Gat-1, The Netherlands. Shell Research BV, Rijswijk, the Netherlands, 11 pp.

Carlson, T. (2019). Petrophysical Report of the Dinantian Carbonates in the Dutch Subsurface (SCAN). Downloadable from: https://www.nlog.nl/sites/default/files/201908/scan_dinantien_petrophysics_report.pdf

Chatziliadou, M. (2009). Rb-Sr Alter und Sr-Pb Isotopencharakteristik von Gangmineralisationen in paläozoischen Gesteinen am Nordrand des linksrheinischen Schiefergebirges (Raum Stolberg-Aachen-Kelmis) und Vergleich mit den rezenten Thermalwässern von Aachen-Burtscheid. Rheinisch-Westfälischen Technischen Hochschule Aachen.

De Ruiter, G. W. M. (1979). Source rock and carbonisation evaluation as well as maceral description of selected samples from well Brouwershavens Gat-1, The Netherlands. Shell Research BV, Rijswijk, the Netherlands, 6 pp.

Kampschulte, A., and Strauss, H. (2004). The sulfur isotopic evolution of Phanerozoic seawater based on the analysis of structurally substituted sulfate in carbonates. Chemical Geology, 204, 255-286.

Pickard, N. A. H., and Gutteridge, P. (1997). Dinantian depositional systems and exploration potential: offshore and onshore, The Netherlands. Sedimentological study. Cambridge Carbonates report for NAM, 596 pp.

Reijmer, J. J., Ten Veen, J. H., Jaarsma, B., and Boots, R. (2017). Seismic stratigraphy of Dinantian carbonates in the southern Netherlands and northern Belgium. Netherlands Journal of Geosciences, 96, 353-379. https://doi.org/10.1017/njg.2017.33

Schroot, B. M., Van Bergen, F., Abbink, O. A., David, P., Van Eijs, R., and Veld, H. (2006). Hydrocarbon potential of the Pre-Westphalian in the Netherlands on- and offshore. TNO report NITG 05-155-C, 421 pp.

Van den Nouland, C. T. J. (2000). Evaluation of the Carboniferous (Namurian) Intervals in wells: WSK-1, MSL-1, STW-1, KTG-1 and BHG-1 for NAM, 33 pp.

Wilpshaar, M., and Van Dijk, C. P. J. (1998). XRF analysis of 4 samples from well Brouwershavensegat-1 for NAM, 4 pp.

1.2.1 Logs

This well has a complete suite of logs (Figure 1-2) and has been petrophysically evaluated within the frame of the SCAN project (Carlson, 2019).

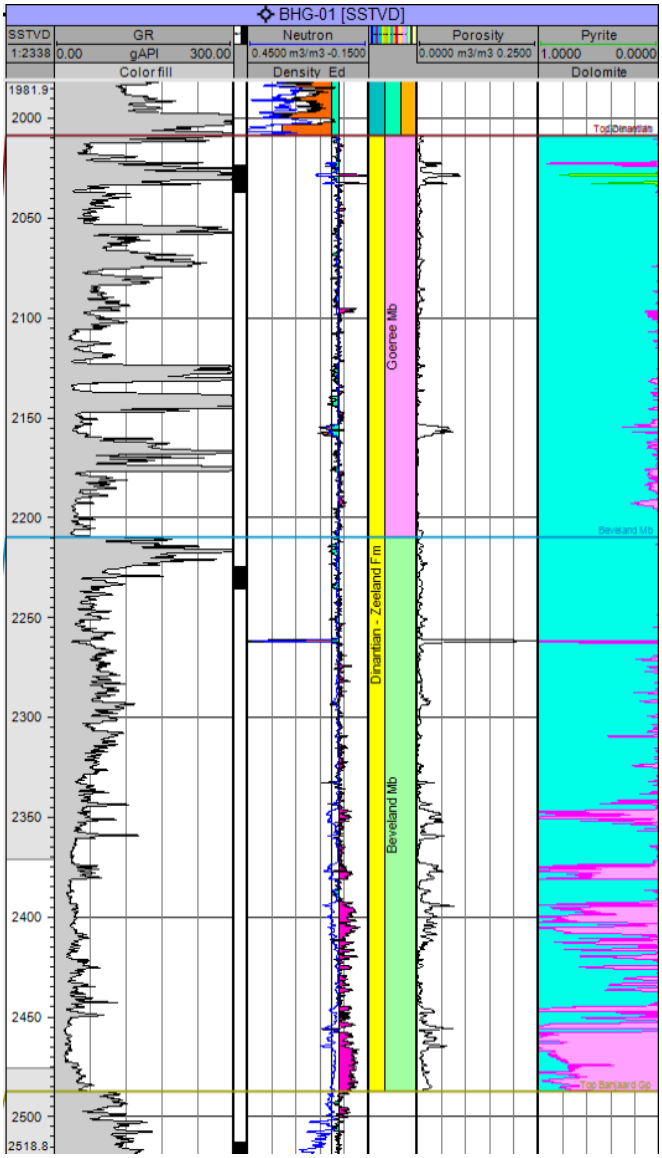

Figure 1-2: Gamma ray, neutron/density, porosity and mineralogical logs in the BHG-01 well.

1.2.2 Cores, sidewall cores and cuttings

Two cores were acquired in the Dinantian interval (Core 1 and 2), at 2168-2182 and 2375-2387 m (MD), respectively.

Core 2 is a thickly bedded well-sorted peloid-intraclast grainstone with some micritised ooids. Bioclast include palaeoberesellids, echinoderms, brachiopods, molluscs, calcispheres and ostracods. Tabulate corals and gastropod moulds are rare. Bedding surfaces are very rare with occasional scoured surfaces marked by concentrations or alignment of bioclasts or coated grains of bioclasts. A micritic hardground or possible exposure surface is present. The succession was deposited in a high energy shallow inner ramp above normal wave base.

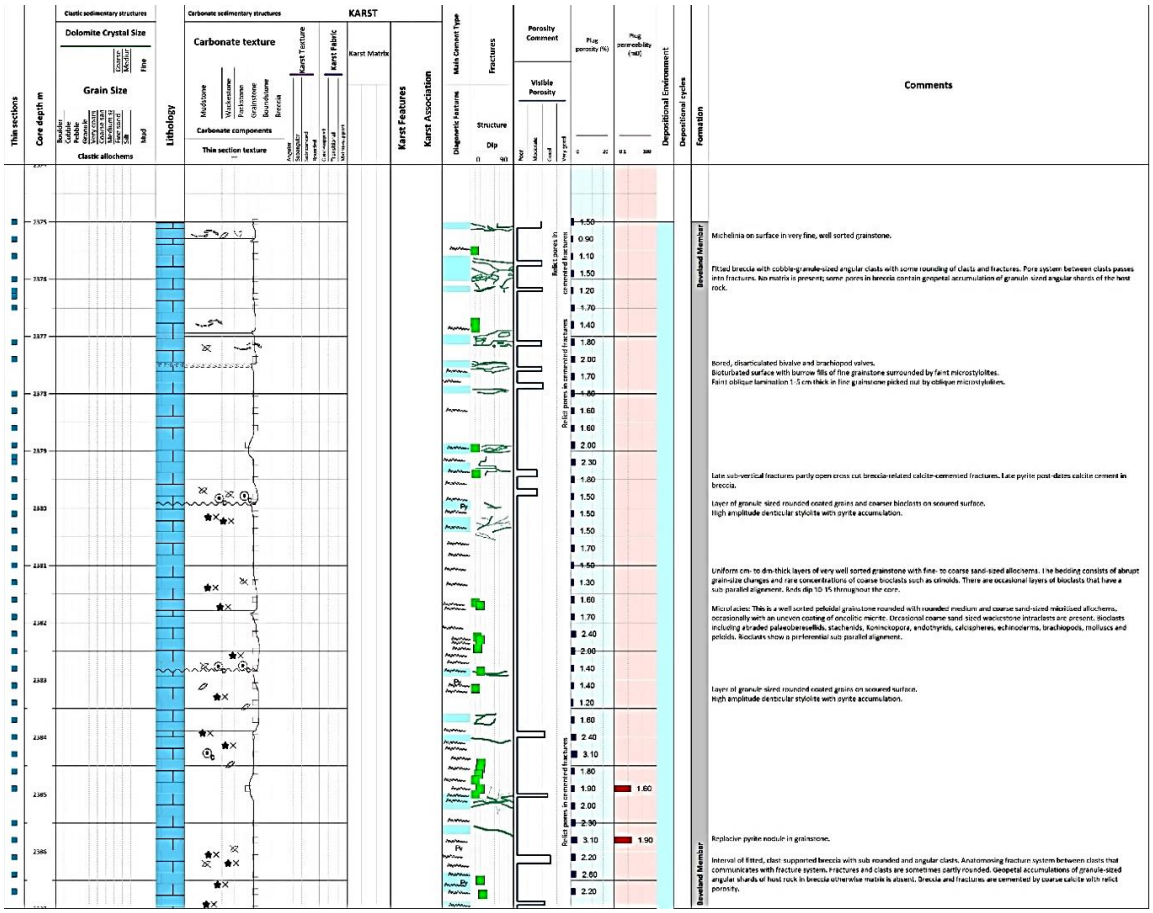

Figure 1-3: Overview of the sedimentological log constructed for Core 2, well BHG-01 (an image of higher resolution is available in Appendix B).

Figure 1-4: Left and right, grainstone with fractures and breccia textures cemented by calcite (Core 2, 2377.10 and 2375.9 m).

Core 1 consists of pebble- to boulder-sized mainly clast-supported limestone breccio-conglomerates with clasts of bioclast wackestone with whole fenestrate bryozoans and stromatactoid cavities; these were probably derived from carbonate mud mounds associated with the shelf margin. Some clasts of bioclast wackestone/packstone are also present; were probably derived from a platform interior setting. The matrix of the breccio-conglomerates comprises dark siliciclastic mudstone, that sometimes occurs as stylolitic concentrations between clasts. A matrix of layered bioclastic grainstone is also occasionally present. An interval of very poorly sorted matrix-rich breccia contains granule- to fine pebble-sized clasts that include dark siliciclastic mudstone. The matrix of the breccia consists of pale grey carbonate muds. This is interpreted as a cave fill or cave collapse breccia with the clasts sourced from the surrounding host limestone and the host matrix represent marine and terrestrial infills.

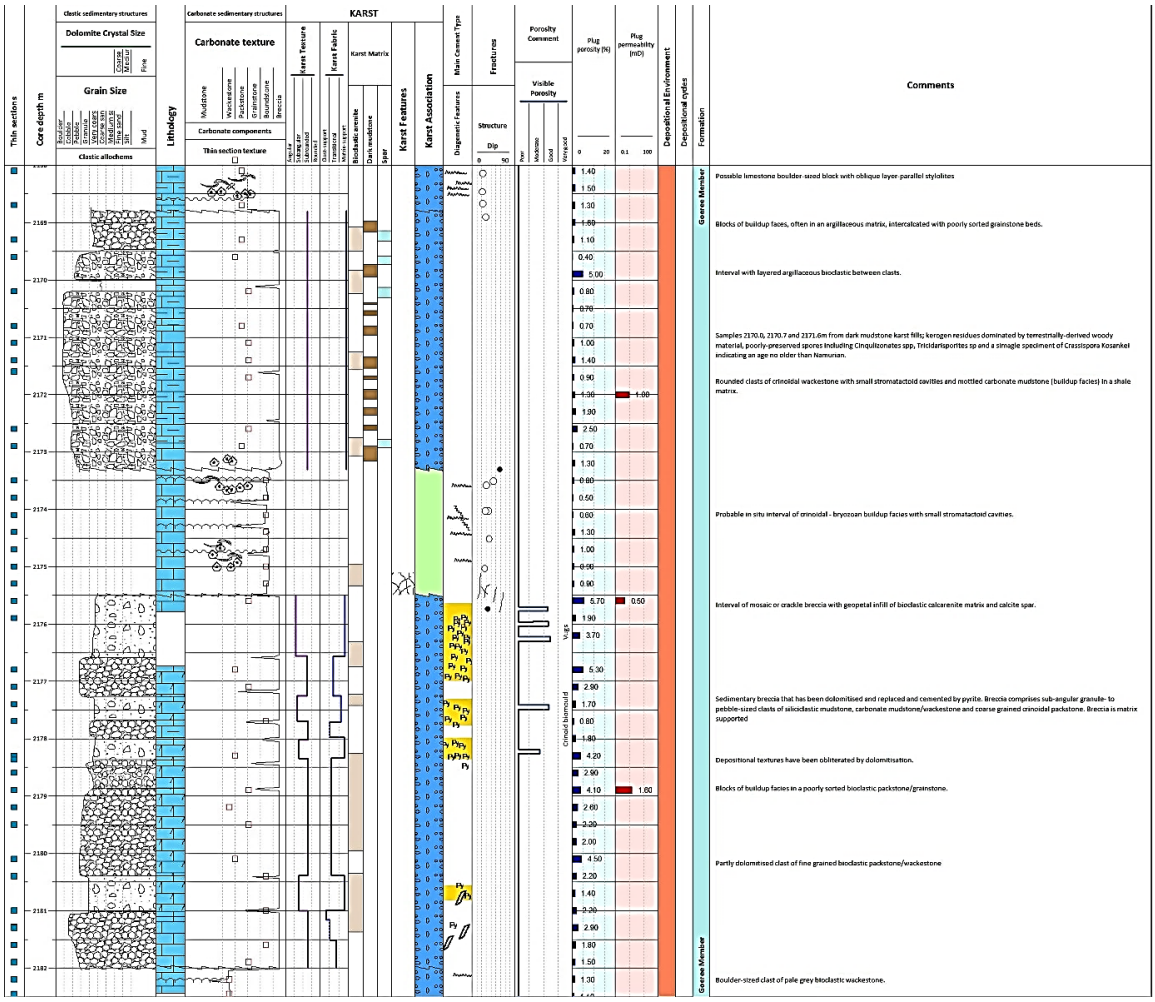

Figure 1-5: Overview of the sedimentological log constructed for Core 1, well BHG-1 (an image of higher resolution is available in Appendix B).

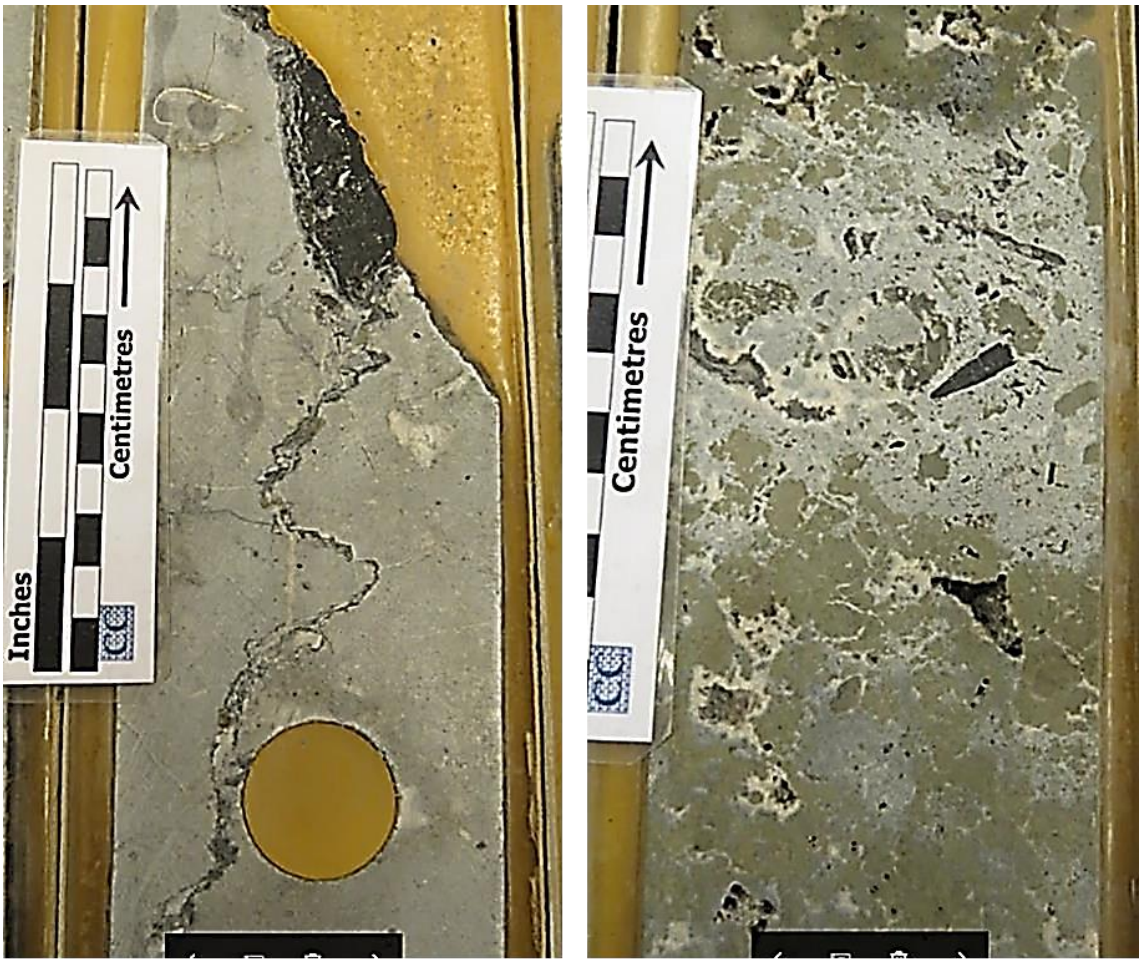

Figure 1-6: Left, clasts of limestone with dark mudstone matrix (Core 1, 2171.6 m). Right, matrix-supported breccia with angular clasts with pervasive replacement by pyrite (Core 1, 2176.2 m).

1.2.3 Petrography and additional analyses

A total number of 76 thin sections are available for this well on which the petrography analysis was performed. Additional analyses were performed during SCAN project. These analyses include:

Biostratigraphy: Mudstone matrix of Core 1 was sampled for dating and as assessment of thermal maturity from spore colouration as follows:
Samples (dark grey colour) from 2170.0 m, 2170.70 m and 2171.60 m. All three samples yielded kerogen residues dominated by terrestrially derived woody material. Miospores are very rare and poorly preserved. The most productive sample is that at 2170.0 m. The very poor assemblage recorded rare *Cingulizonates* spp., ?*Tricidarisporites* sp. and a single specimen very tentatively identified as *Crassispora kosankei*, providing very limited evidence for an age not older than Namurian.

Spore Colour: The obtained spore colour is very dark brown/black. Equivalent to 3.7 (Staplin 1977, text Figure 10).

Cathodoluminescence (CL): A total of five thin sections were examined for their CL pattern, two of which correspond with fluid inclusion samples, and three from mineralised karst breccia in Core 1.

Fluid inclusions: One sample from mineralised karst breccia in Core 1 and one sample from the calcite-cemented fracture in Core 2 (the results are summarised in Section 1.7.4).

Carbon and oxygen isotopes: A total of seven samples were analysed for their stable C and O isotopic composition (Table 1-5). The samples were taken from fracture fill cements and bulk matrix. The aims of this sampling were as follows:

- Core 1: To characterise the diagenetic conditions of cementation in sub-Limburg karst and subsequent mineralisation.
- Core 2: To characterise the diagenetic conditions of cementation in hydrofractures.

Stable Sulphur isotopes ($\delta^{34}S$): Two samples from pyrite in mineralised karst breccia in Core 1 and one sample from the pyrite dispersed in limestone matrix from Core 2 were analysed for their Sulphur isotopes. The obtained results are summarised in Table 1-2.

Table 1-2: Overview of the results of stable Sulphur isotope analyses performed on the BHG-01 well (SCAN project).

Depth (m)	Sample	$\delta^{34}S_{V\text{-}CDT}$
2375.15	Pyrite in limestone matrix	-29.14
2178.37	Pyrite in mineralised karst breccia	+15.10
2178.1	Pyrite in mineralised karst breccia	+17.83

Vitrinite reflectance (%Rr): Two samples from the intervals of Core 1 with apparently high organic material were analysed for their %Rr . The obtained results are summarised in Table 1-3.

Table 1-3: Available vitrinite reflectance measurements for the BHG-01 well.

Depth (MD)	Measurement type	%Rr	Source
1478	Vitrinite reflectance (random, mean) - %Rr	0.89	TNO-NITG
1700	Vitrinite reflectance (random, mean) - %Rr	0.86	TNO-NITG
2198	Vitrinite reflectance (random, mean) - %Rr	0.96	TNO-NITG
2198	Vitrinite reflectance (maximum, mean) - %Rmax	2.58	TNO-NITG
2398	Vitrinite reflectance (random, mean) - %Rr	1.64	TNO-NITG
2398	Vitrinite reflectance (maximum, mean) - %Rmax	1.95	TNO-NITG
2888	Vitrinite reflectance (random, mean) - %Rr	1.73	TNO-NITG
2372	Vitrinite reflectance (maximum, mean) - %Rmax	1.90	TNO-NITG
1474	Vitrinite reflectance - %Ro	1.03	
1478	Vitrinite reflectance - %Ro	1.00	
2170	Vitrinite reflectance - %Ro	2.49	SCAN project
2171.6	Vitrinite reflectance - %Ro	2.31	SCAN project

1.3 Stratigraphy

The successions of the Brouwershavense Gat-1 well spans from Quaternary to the Devonian, encountering the Cretaceous unconformity at 1398 m (MD) over the Namurian and the Dinantian at 2153 m (MD).

Table 1-4: Stratigraphy of the BHG-01 well (from www.nlog.nl).

Stratigraphic unit	Top interval	Base interval
QUATER. UNDIFF.	0	40
Maassluis Fm.	40	95
Oosterhout Fm.	95	197
Rupel Clay Mb.	197	341
Vessem Mb.	341	359
Asse Mb.	359	513
Brussels Sand Mb.	513	584
Ieper Member	584	837
Basal Dongen Sand Mb.	837	872
Landen Clay Mb.	872	929
Ommelanden Fm.	929	1398
Baarlo Fm.	1398	1748
Ubachsberg Mb.	1748	1788
Epen Fm.	1788	2153
Goeree Mb.	2153	2360
Beveland Mb.	2360	2646
Bosscheveld Fm.	2646	2675
Bollen claystone Fm. (Devonian)	2675	2906

1.3.1 Dinantian interval

In the current study the original interpretation of the lithostratigraphy follows the terminology of Van Adrichem Boogaert and Kouwe (1994) with the Zeeland Formation made up of the Beveland and Goeree Members. However, the Beveland Member has been replaced by sequence stratigraphic units described below and the Goeree Member is re-interpreted as an interval of karst collapse in the BHG-01 well.

1.4 Microfacies

The following textures (Figure 1-7) were noted as the original depositional facies in the BHG-01 well:

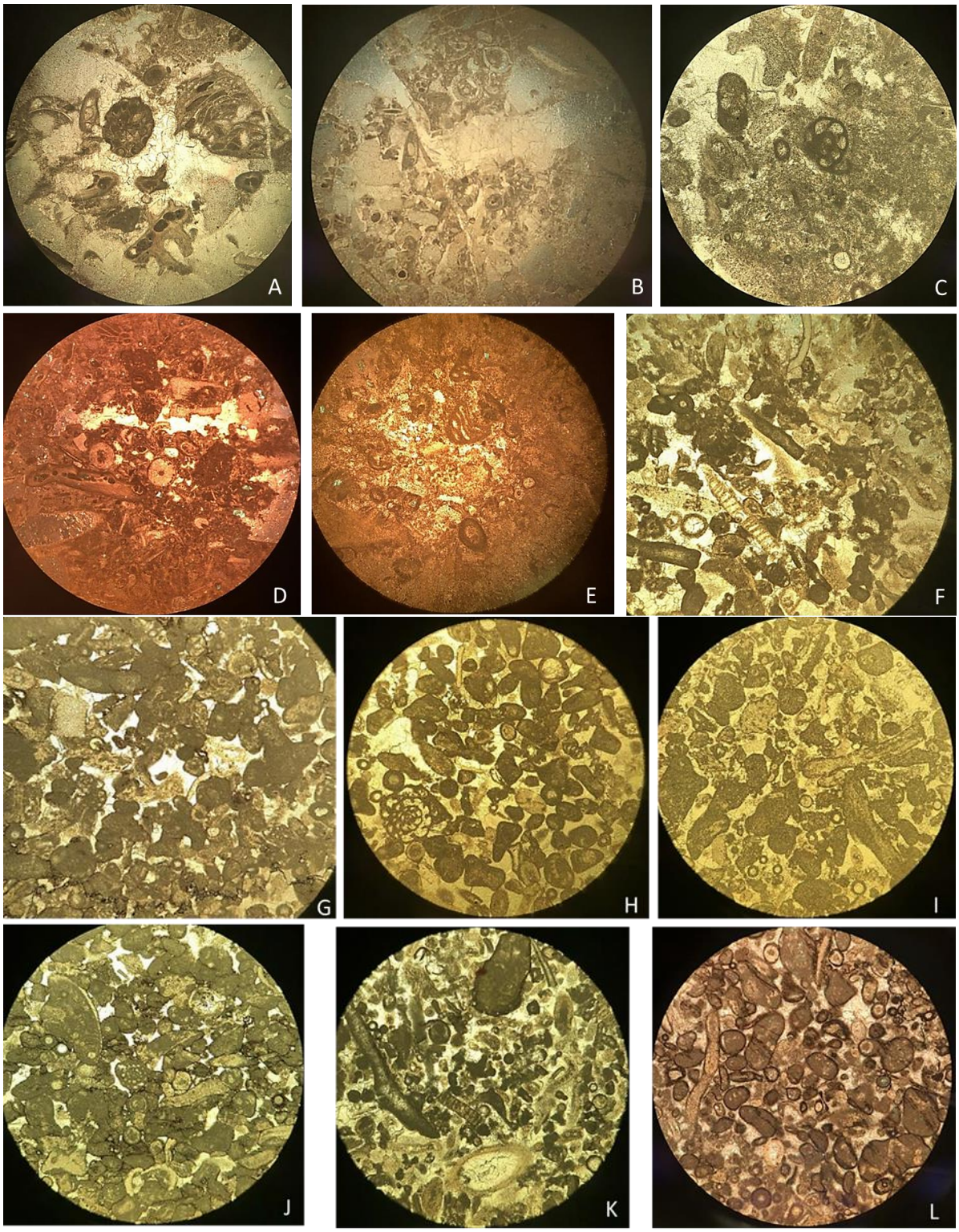

Figure 1-7: Representative photomicrographs of the facies types observed in the BHG-01 well. A) Crinoidal-fenestrate bryozoan pack- to grainstone (2169.3 m, PPL. FOV 4 mm). B) Crinoid-fenestrate bryozoan packstone/grainstone (2170.2 m, PPL. FOV 8 mm). C) Bioclastic packstone with micropeloidal micrite matrix (2173.8 m, PPL. FOV 2 mm). D) Bioclastic-crinoidal wackestone with small stromatactoid cavities and a micropeloidal micrite matrix (2174.7 m, PPL. FOV 8 mm). E) Bioclastic wackestone/packstone (2179.2 m, PPL. FOV 4 mm). F) Algal-foraminiferan-peloid grainstone (2375.3 m, PPL. FOV 3 mm). G) Well sorted, well rounded, bioclastic-peloidal grainstone (2375.6 m, PPL. FOV 3 mm). H) Well rounded, peloidal-algal-foraminiferan-grainstone (2376.0 m, PPL. FOV 4 mm). I) Well sorted, well rounded, foraminiferan-bioclastic-peloidal grainstone (2377.4 m, PPL. FOV 4 mm). J) Poorly sorted peloid bioclastic-intraclast-peloidal grainstone

(2378.3 m, PPL. FOV 4 mm). K) Sorted bioclastic (algal)-peloidal-intraclast grainstone (2379.5m PPL. FOV=4mm). L) Well rounded, well sorted, peloidal-bioclastic intraclast grainstone (2380.7 m, PPL. FOV 4 mm).

1.5 Biostratigraphy

Core 1: Foraminiferal assemblages indicate a V3b to V3c (Warnantian) age for the host limestone. This would be equivalent to the Late Asbian and Brigantian in the UK. The mudstone karst fills (samples from 2170.0 m 2170.70 m and 2171.60 m) yielded kerogen residues dominated by terrestrially derived woody material. Miospores are very rare and poorly preserved. The most productive sample is that at 2170.0 m. The very poor assemblage recorded included rare *Cingulizonates* spp., ?*Tricidarisporites* sp. and a single specimen very tentatively identified as *Crassispora kosankei*, providing very limited evidence for an age not older than Namurian.

Core 2: A V1a, Cf4α earliest Moliniacian-age is suggested by the microfauna, including *Pachysphaerina* pachysphaerica recovered from Core 1 (Bless, 1978). This core is there considered to be equivalent to Core 9 in S05-01. Moreover, the presence of the problematic algae *Globochaetes* in the thin section prepared from 2381.0 m is indicative of a late Tournaisian Cf3 age.

1.6 Sequence stratigraphy

A total of ten depositional cycles representing the whole of the Dinantian have been recognised in the SW Netherlands; at least four depositional cycles, based on correlations with O18-01, BHG-01 and S05-01, have been recognised in the BHG-01. The upper depositional cycles in the well BHG-01 have not been recognised since it has been overprinted by karst collapse. This collapse is interpreted as a doline collapse.

Cycle 1a (cyan): This depositional cycle represents the initial flooding of the basin; the thin TST has a clean gamma ray signature above the thick high gamma ray fine Tournaisian clastics. This is interpreted as deposition of clean carbonates in shallow water. This is followed by increasing gamma interpreted as deposition of more muddy carbonates in deeper water. The HST has a clean gamma ray signature suggesting that it consists of inner ramp carbonates.

Cycle 1b (pink): This depositional cycle comprises a thin TST with a thick HST interpreted as cyclic shallow to mid-ramp ramp carbonates.

Cycle 1c (orange): This depositional cycle comprises a thick TST with a HST interpreted as cyclic subtidal to peritidal shallow ramp carbonates, probably capped by peritidal facies. Here, a thick TST passing up into a HST that has a moderately high gamma ray signature. Core from the HST intervals in other wells suggests that this depositional cycle consists of cyclic shallow subtidal to peritidal shallow ramp carbonates with cycle tops marked by peritidal facies. The subtidal facies are dominated by oncoids, other coated and highly micritised grains suggesting deposition took place in a relatively restricted shallow carbonate ramp setting.

Cycle 1d (light green): This depositional cycle comprises a thin TST; core from the HST indicates deposition in a high energy inner carbonate ramp setting above normal wave base. The 1d sedimentary cycle has been eroded and is overlain by karst collapse or fill.

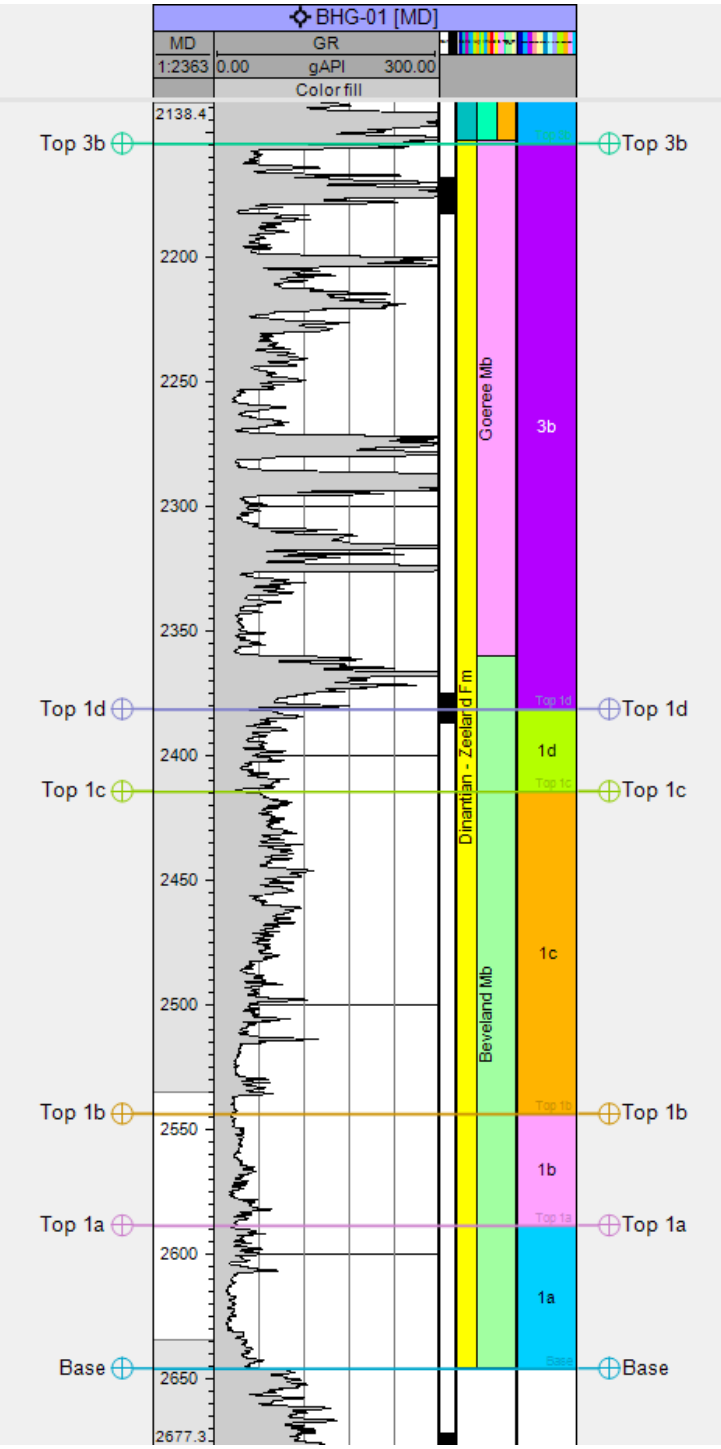

Figure 1-8: Sequence stratigraphic interpretation of the BHG-01 well.

1.7 Diagenesis

1.7.1 Paragenetic sequence

Based on the core observations and available thin sections the following paragenetic sequence was established:

Eogenesis:

1. Grain micritisation and dissolution of aragonite components (Figure 1-9A).

2. Early fenestral vugs associated with intertidal settings (syn-sedimentary) (Figures 1-9B and 1-9C).
3. Fibrous marine cement occurring in vugs, intraparticle pores and shelter cavities (Figure 1-9D).

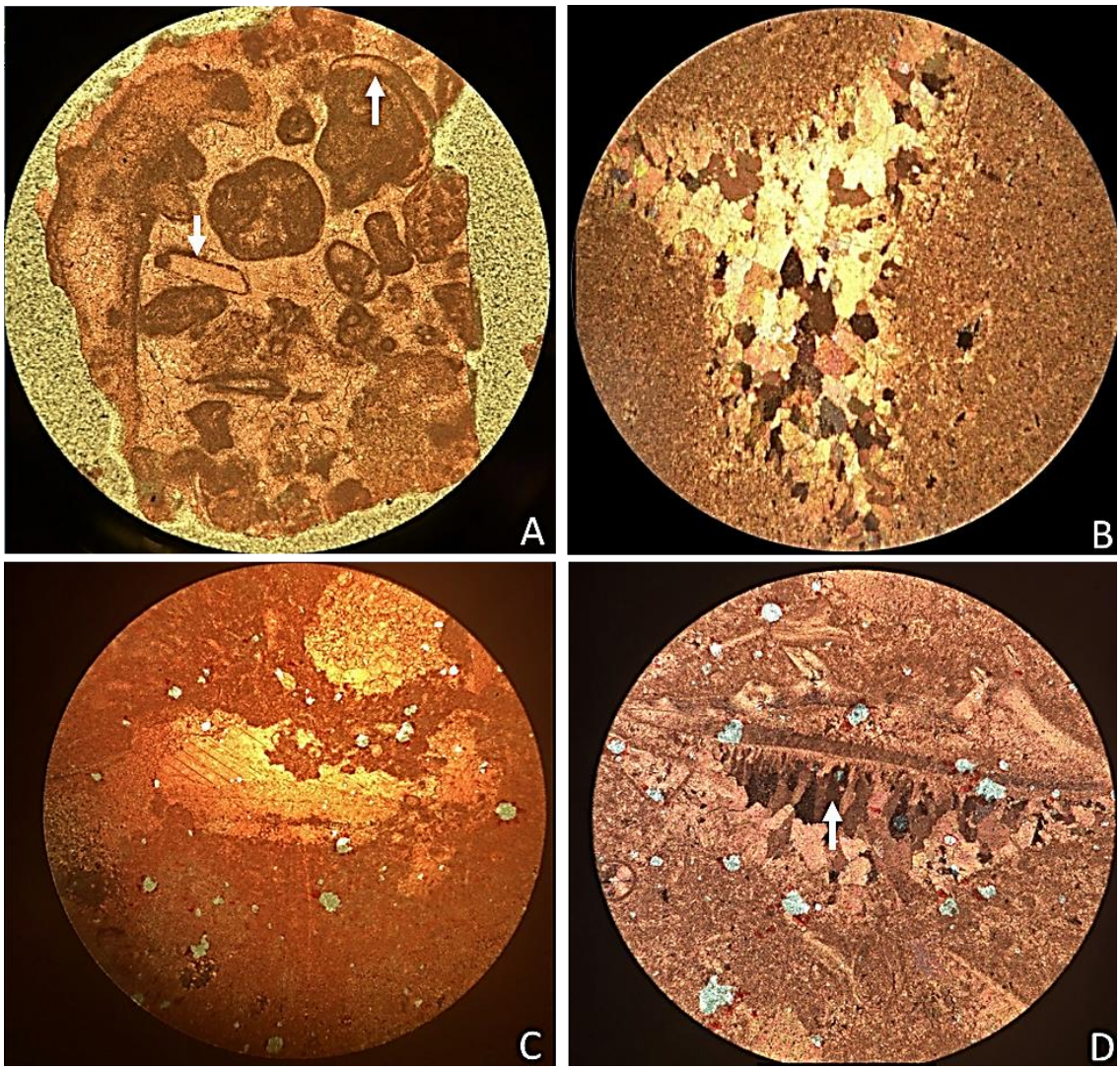

Figure 1-9: Representative photomicrographs of the diagenetic phases interpreted as the eogenetic modifications in the BHG-01 well. A) Grain micritisation and dissolution of aragonitic components (from cuttings 2308 m, PPL. FOV 2 mm). B, C) Early fenestral vugs associated with intertidal settings (syn-sedimentary) (2168.10 m, XPL. FOV 3 mm), (2172.90 m, PPL. FOV 4 mm). D) Fibrous marine cement occurring in vugs (2174.10 m, XPL. FOV 2 mm).

Shallow Burial

4. Calcite cement within the interparticle pore spaces – shallow burial: C1 + C2. Including syntaxial calcite overgrowths.
5. Disseminated pyrite in matrix.
6. Authigenic quartz (relative timing unknown as there are no cross-cutting relationships).

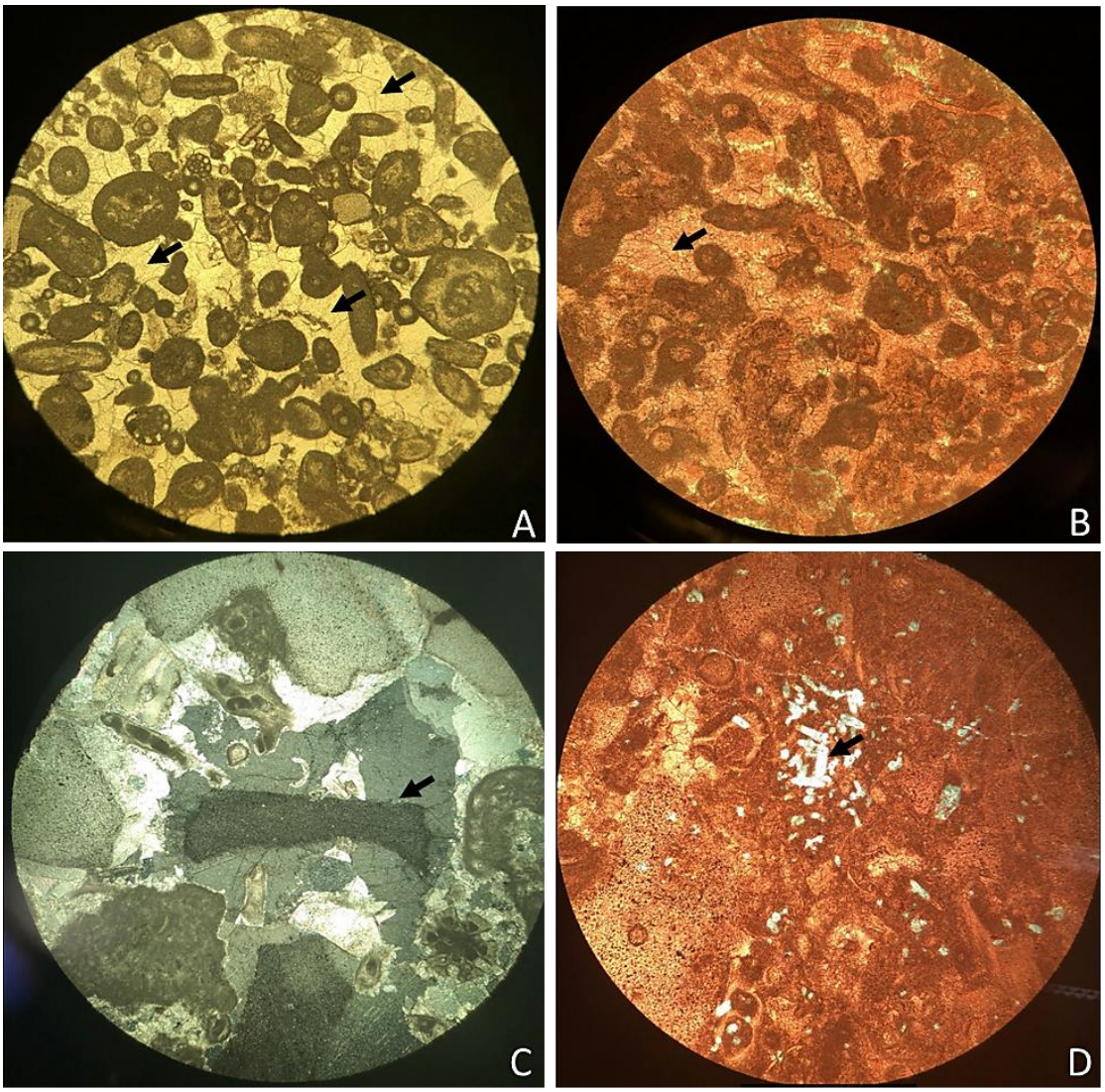

Figure 1-10: Representative photomicrographs of the diagenetic phases interpreted as the shallow burial modifications in the BHG-01 well. A, B) Calcite cement within interparticle pore space (C1) (2378.10 m, PPl. FOV 4 mm), (from cuttings 2308.0 m, PPL. FOV 2 mm). C) syntaxial cement overgrown on a crinoid fragment (C2) (2169.30 m, XPL. FOV 4 mm). D) Authigenic quartz, timing unknown (2169.60 m, PPL. FOV 2 mm).

Telogenesis – Namurian Karst

Karstification clearly pre-dates chemical compaction and high amplitude bed-parallel stylolites.

7. Ragged–edged dissolution enhanced fractures (Figure 1-11A).
8. C3 non-ferroan calcite cement in karst fractures and vugs (no geochemical analysis undertaken) (Figures 1-11B and 1-11C).
9. Ferroan calcite cemented hairline fractures – C3b (predates D2 dolomites) (Figures 1-11D to 1-11F).

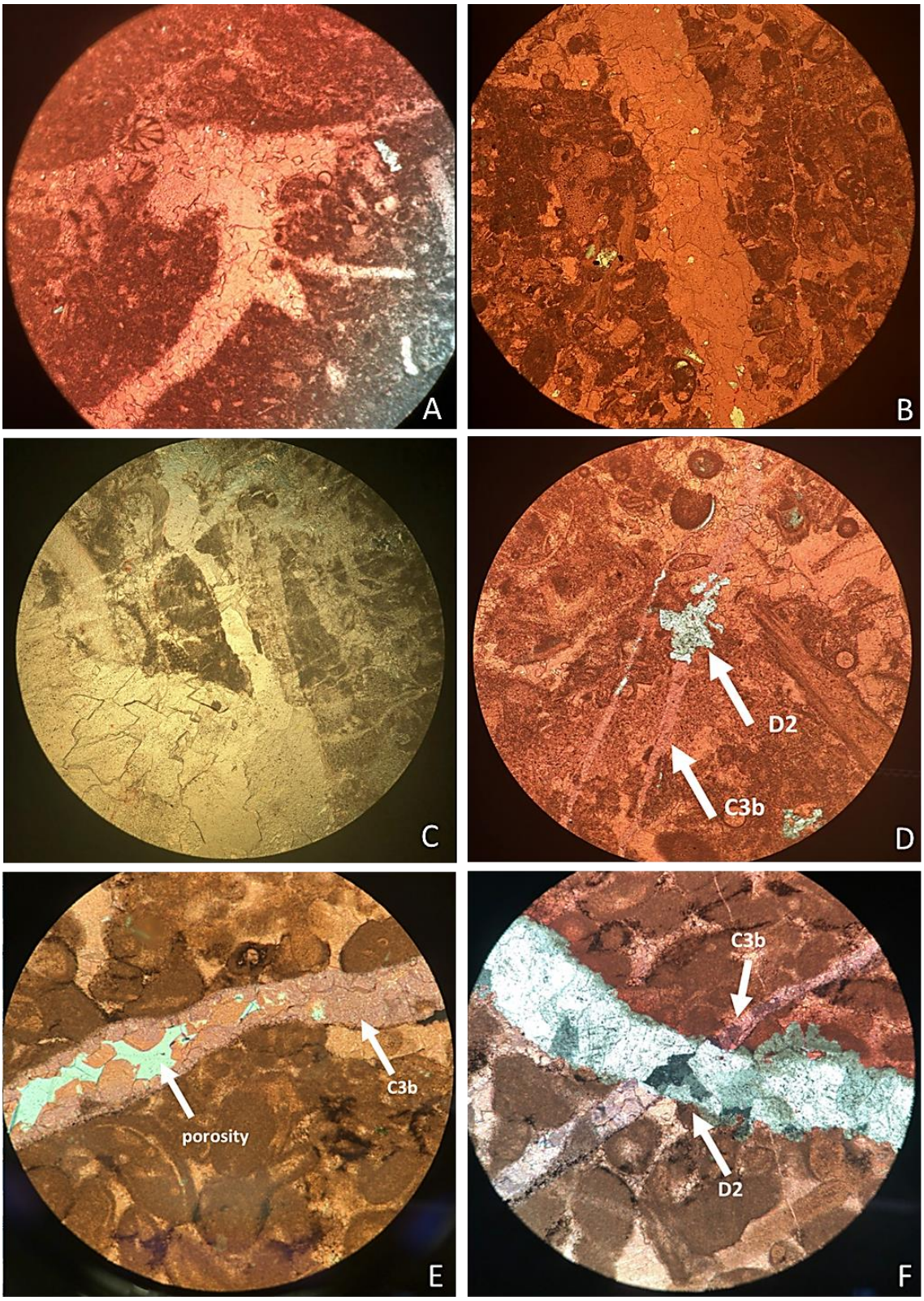

Figure 1-11: Representative photomicrographs of the diagenetic phases interpreted as telogenesis and karstification modifications in the BHG-01 well. A) Ragged–edged dissolution enhanced vug (2173.50 m, PPL. FOV 4 mm). B, C) Calcite cement (non-ferroan) C3 in fractures (2174.40 m, PPL. FOV 4 mm), (2170.20 m, PPL. FOV 4 mm). D, E, F) Ferroan calcite cemented hairline fractures – C3b? (predates D2 dolomites), (2173.80 m, PPL. FOV 2 mm), (2181.60 m, PPL. FOV 2 mm), (2181.60 m, XPL. FOV 2 mm).

Burial – Mineralisation of the Namurian Karst

10. D2 dolomite replacement and dolomite cement in fractures. Postdates C3 calcite cemented fractures. D2 saddle dolomites also occur as cement along stylolites (Figures 1-12 and 1-13).
11. Pyrite (Figure 1-14).
12. Galena and Sphalerite (Figures 1-14 and 1-15).
13. Chemical compaction – stylolites – possibly postdates D2 dolomites (concentrated along stylolites often) (Figure 1-13).
14. Non-ferroan, poikilotopic calcite cement in vugs: C4. Rare fracture postdating dolomite cemented by calcite (Figure 1-16).
15. Barites (Figure 1-16).

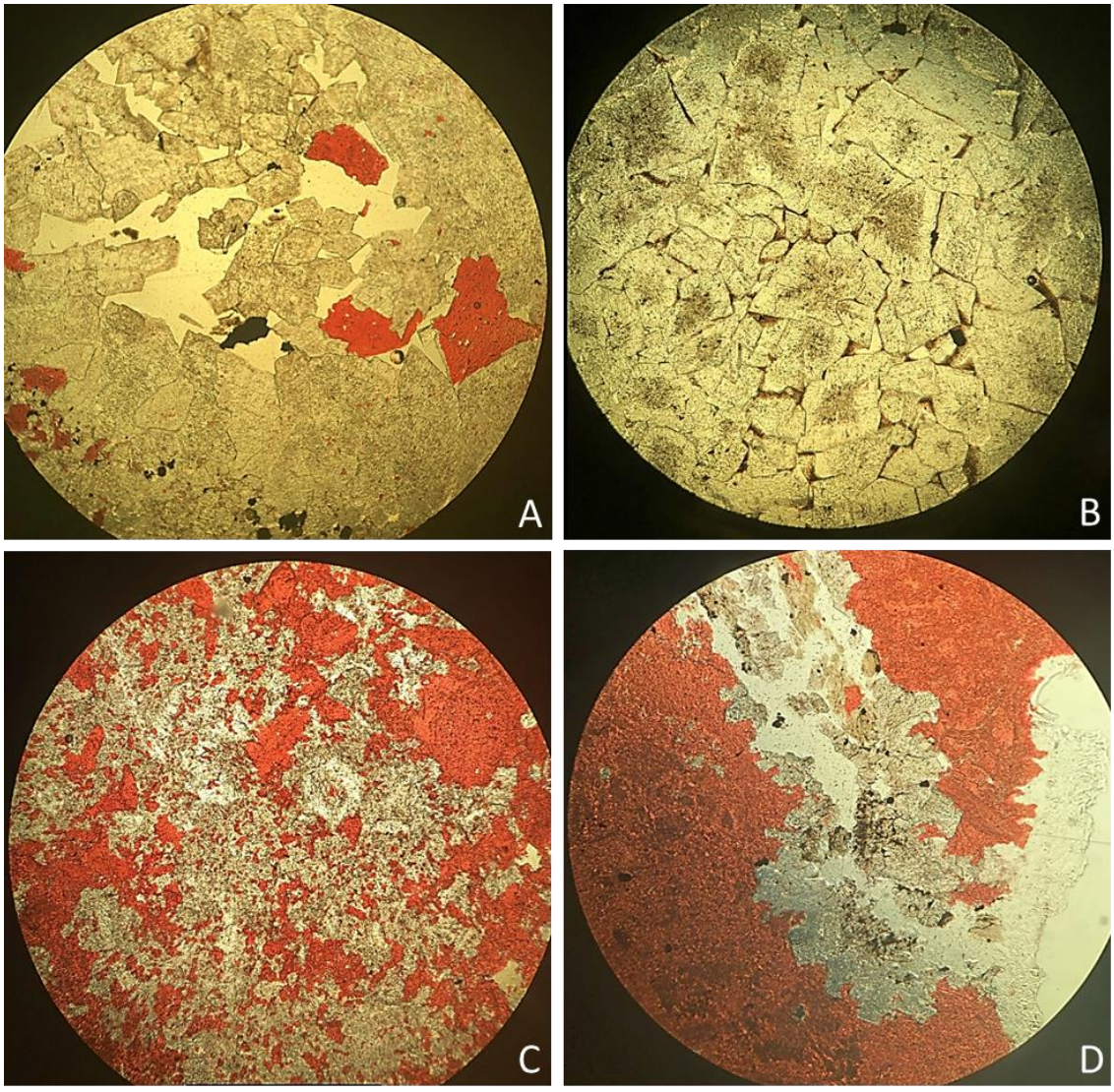

Figure 1-12: Representative photomicrographs showing D2 dolomite replacement and dolomite cement in fractures of the BHG-01 well. A) Vuggy porosity associated with dolomite cements. Note that the porosity is partially filled by calcite cement (2177.40 m, PPL. FOV 4 mm). B) Coarse dolomite crystals with minor inter-crystalline porosity (2178.60 m, PPL. FOV 2mm). C) Patchy replacement dolomites (2177.40 m, PPL. FOV 4 mm). D) Dolomite cementing a fracture. Note the remnant porosity in fracture (2172.60 m, PPL. FOV 2 mm).

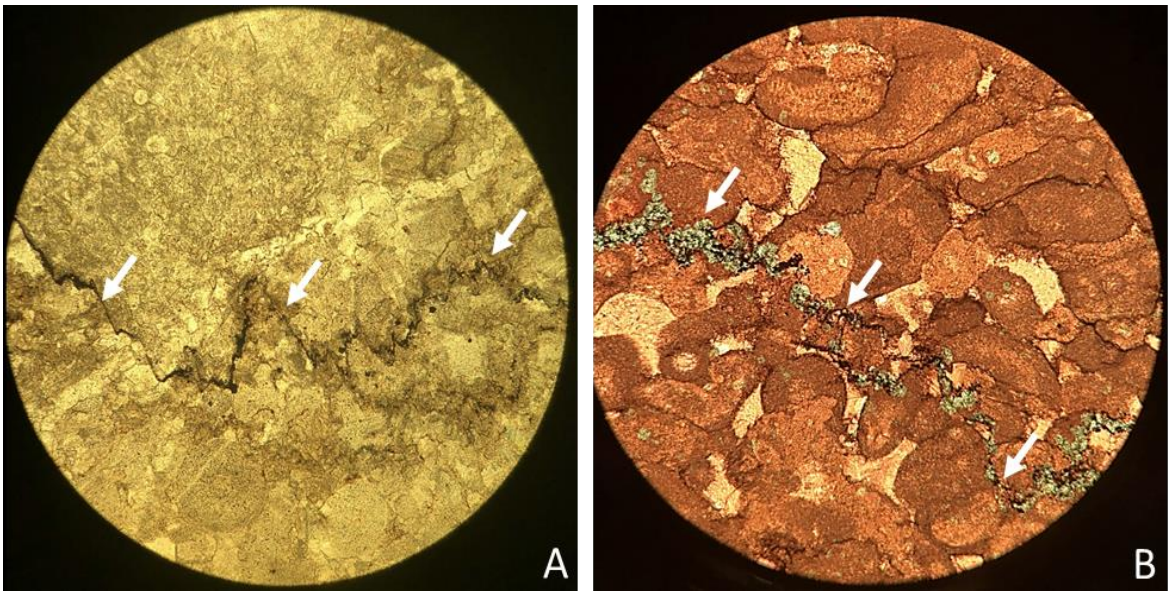

Figure 1-13: Representative photomicrographs showing the cross-cutting relationship between dolomitisation and bed-parallel stylolites in the BHG-01 well. A) A bed-parallel stylolite postdating dolomite (2181.90 m, PPL. FOV 4 mm). B) D2 dolomite focused along a bed-parallel stylolite (2378.30 m, PPL. FOV 2 mm).

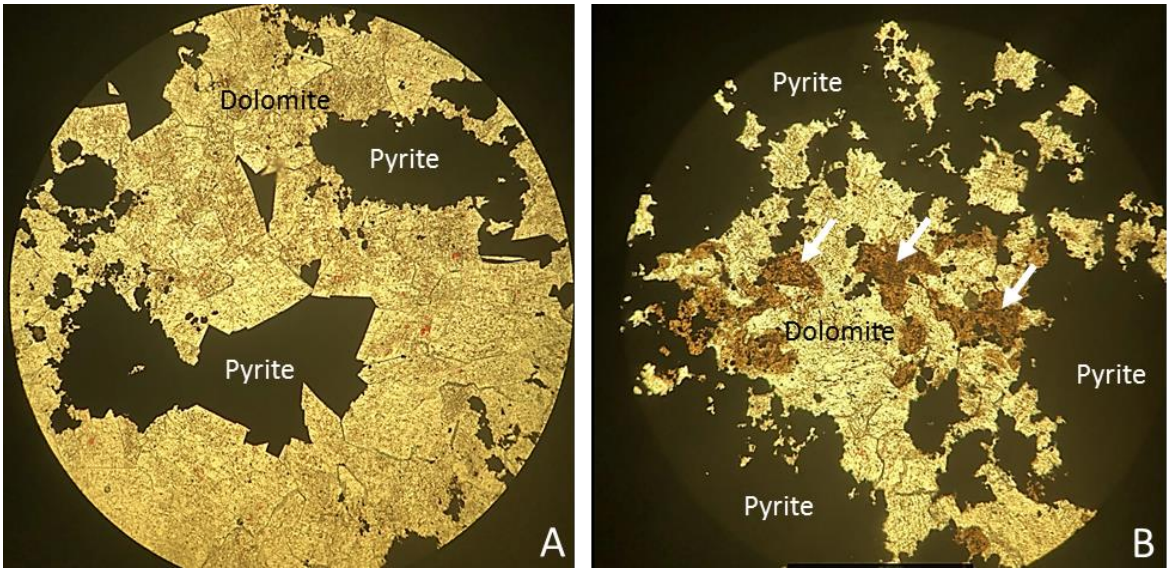

Figure 1-14: Representative photomicrographs showing pyrite and mineralisation in the BHG-01 well. A) Pyrite postdating dolomites (2175.90 m, PPL. FOV 4 mm). B) Sphalerite (white arrows) and pyrite in a background of dolomite (2175.90 m, PPL. FOV 2 mm).

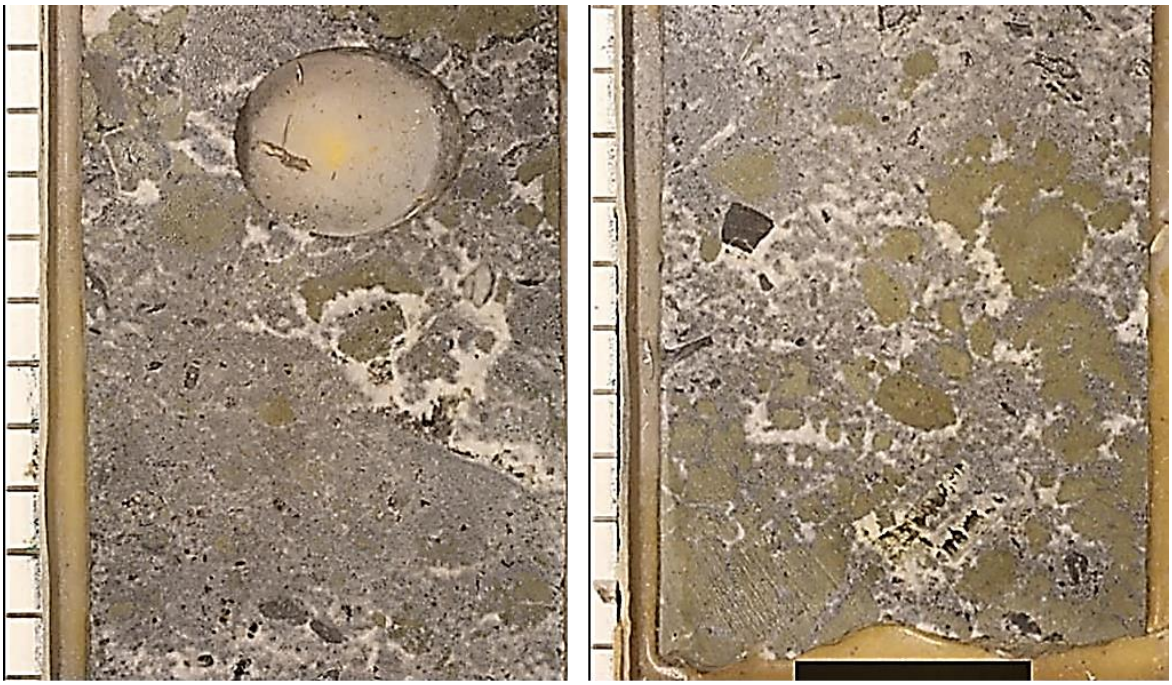

Figure 1-15: Core scale (Core 1; 2171.4 m and 2171.6 m) image showing mineralisation of the Namurian karst in the BHG-01 well.

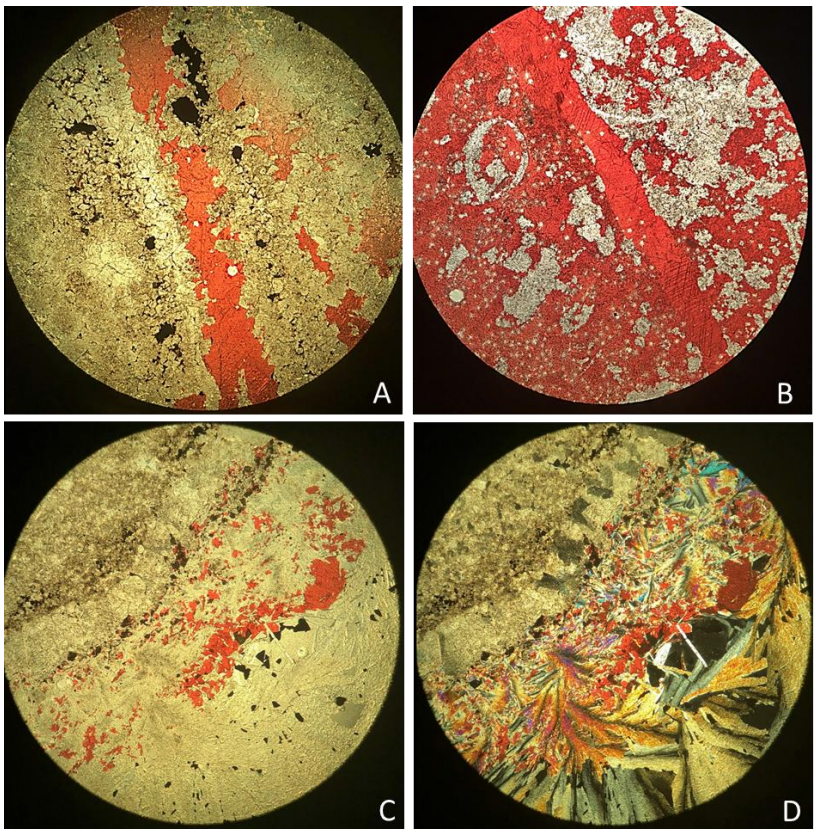

Figure 1-16: Representative photomicrographs showing non-ferroan, poikilotopic calcite cement (C4) and barite mineralisation in the BHG-01 well. A) D2 dolomite is lined by pyrite and poikilotopic calcite cement (C4) is the final cement phase (pink) (2178.60 m, PPL. FOV 4 mm). B) Fracture cross-cutting D2 dolomite, cemented by C4 calcite (2180.40 m, PPL. FOV 4 mm). C, D) Replacement dolomites (D2), followed by pyrite and C4 calcite (pink). Barite laths appear to postdate both phases (2181.3 m, PPL. and XPL. FOV 8 mm).

Burial – Hydrofracturing

This phase of burial diagenesis postdates mineralisation of karst and saddle dolomite cementation. The hydrofracturing results in shards of angular host rock, with horizontal to sub-horizontal breccia fabrics. The breccia comprises angular clasts that often show a fitted fabric with adjacent clasts and adjacent fracture walls. There is sometimes a geopetal accumulation of angular granule- to pebble-sized clasts between coarser clasts at the base brecciated zone. These breccias are all cemented by late pyrite and calcite. This burial stage includes:

17. Fracturing.
18. Late pyrite lines fractures.
19. Coarse non-ferroan calcite cements breccia porosity, but some remnant porosity often remains as bridge porosity.

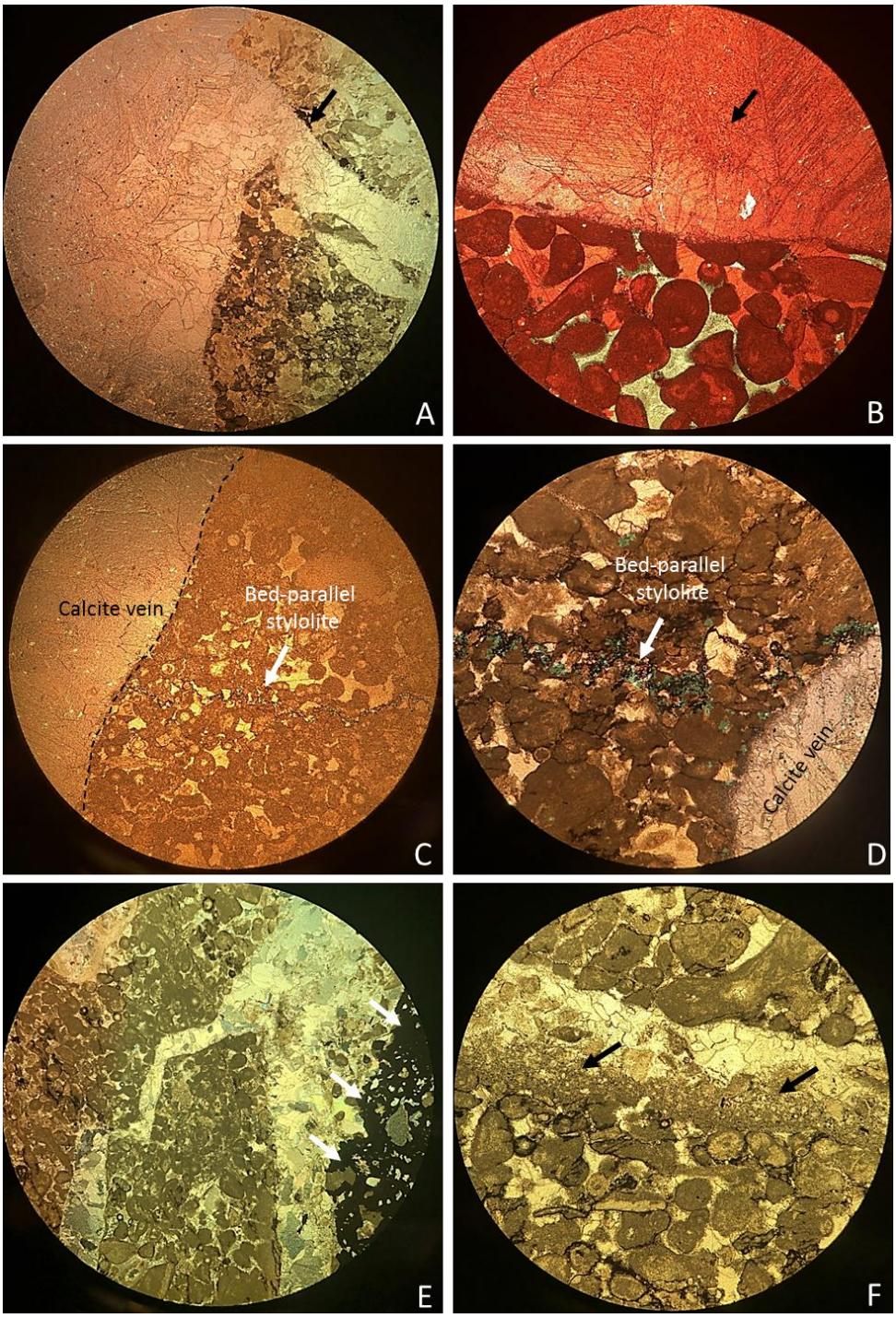

Figure 1-17: Representative photomicrographs showing fracturing, calcite cementation and the late pyrite mineralisation in the BHG-01 well. A) Fractures cemented by blocky calcite with some pyrite locally lined along the fracture wall (black arrow) (2378.60 m, PPL. FOV 8 mm). B) Blocky calcite cement (2169.30 m, PPL. FOV 4 mm). C) Calcite vein postdating a bed-parallel stylolite (2376.5 m, PPL. FOV 4 mm). D) Calcite vein postdating a bed-parallel stylolite which is lined by dolomite (2386.40 m, PPL. FOV 4 mm). E) Calcite cemented fractures. Note the pyrite nodule indicated by the white arrows (2380.10 m, PPL. FOV 8 mm). F) Geopetal sediment fill at the base of fracture indicated by the white arrows (2386.1 m, PPL. FOV 4 mm).

1.7.2 Cathodoluminescence (CL)

Samples selected for further diagenetic analysis can be split up into two groups, i.e. calcite cemented hydrofractures (samples 2377.25 m and 2379.10 m), dolomitised and mineralised karst breccias (samples 2178.10 m, 2178.37 m and 2181.07 m).

Calcite cemented hydrofractures (samples 2377.25 m and 2379.10 m): The hydrofractures cemented by two different calcite phases.
The vein in 2377.25 m is cemented by dull luminescent calcite (Figures 1-18A to C). The calcite crystals in the vein can be followed across the fracture wall into the matrix suggesting recrystallisation of the host rock may have occurred calcite (Figures 1-18E to F).
In sample 2379.10 m the calcite cement consists of alternating bands of ferroan and non-ferroan calcite. The ferroan calcite has a purple stain and is non-luminescent, while the non-ferroan calcite stained pink and is dull-bright luminescent (Figures 1-19A to D). This calcite phase pre-dates the non-luminescent dolomite (Figures 1-19A and B).
Dolomitised and mineralised karst breccias (samples 2178.10, 2178.37 and 2181.07): The dolomite crystals are generally anhedral and dull luminescent. Small dolomite crystals replace the precursor matrix and large saddle dolomite veins occur in veins and pores (Figures 1-19E and F). Brighter luminescent zones can be observed in the saddle dolomite crystals and the last dolomite stage is non-luminescent. In some samples the bright luminescent zones is more clearly developed (Figures 1-20A to 1-20D). Locally a minor phase of dissolution and recrystallisation pre-dates the non-luminescent dolomite (Figures 1-20C to 1-20F).
The dolomite is postdated by dull to bright luminescent calcite cement (Figures 1-21A and 1-21B). In some samples the dolomite is corroded and replaced by this calcite (Figures 1-21C and 1-21D) whereas in others it preferentially replaced crinoids (Figures 1-21E and 1-21F).
Pyrite cubes are associated with both dolomite and calcite cements (Figures 1-21A and 1-21B).

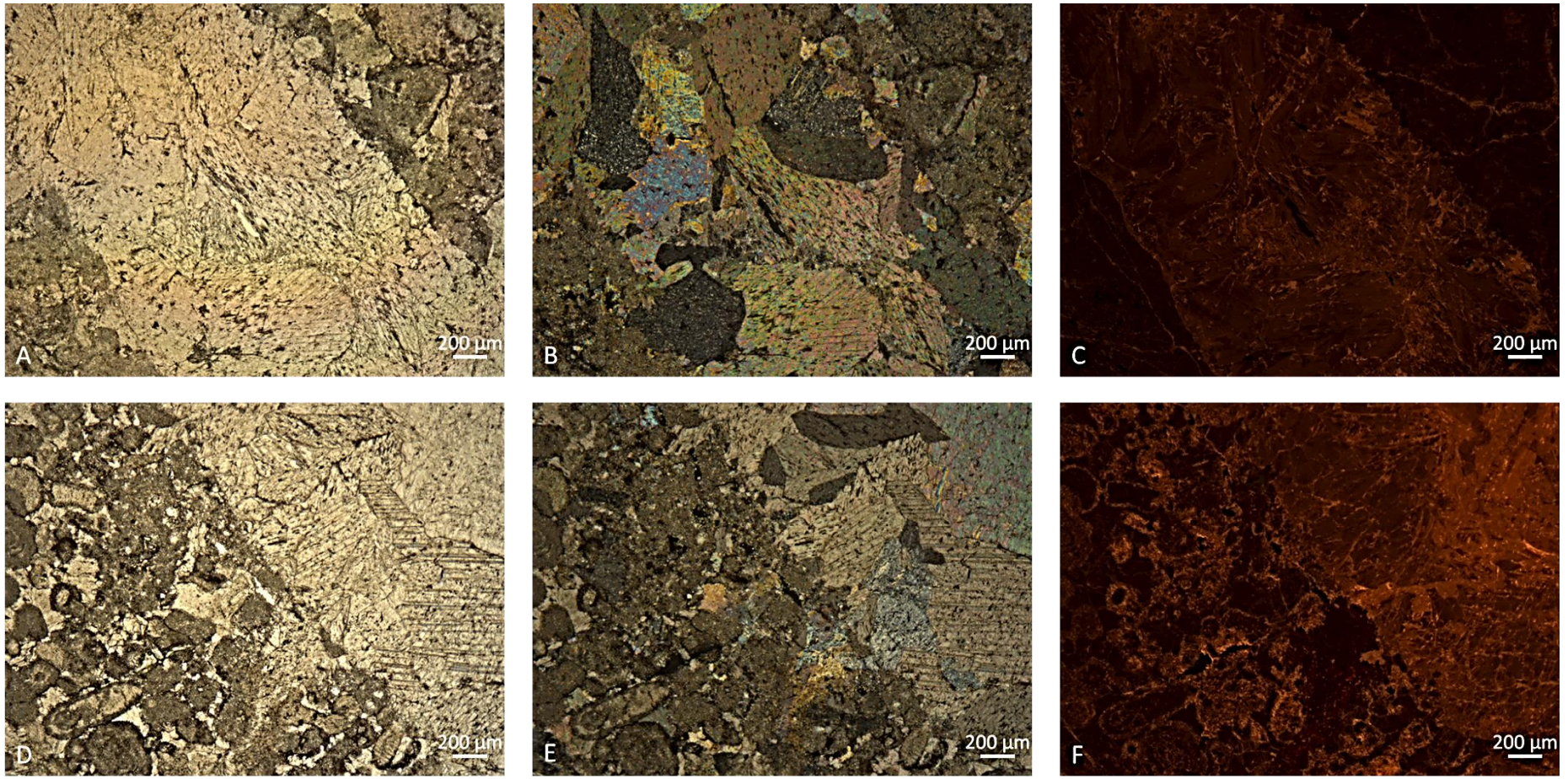

Figure 1-18: Equivalent PPL, CPL and CL microphotographs. A – C) The hydrofractures are cemented by a fairly dull luminescent calcite (2377.25 m). D – F) A crystallographic continuity between calcite crystals occurring in the vein and the matrix can be observed (2377.25 m).

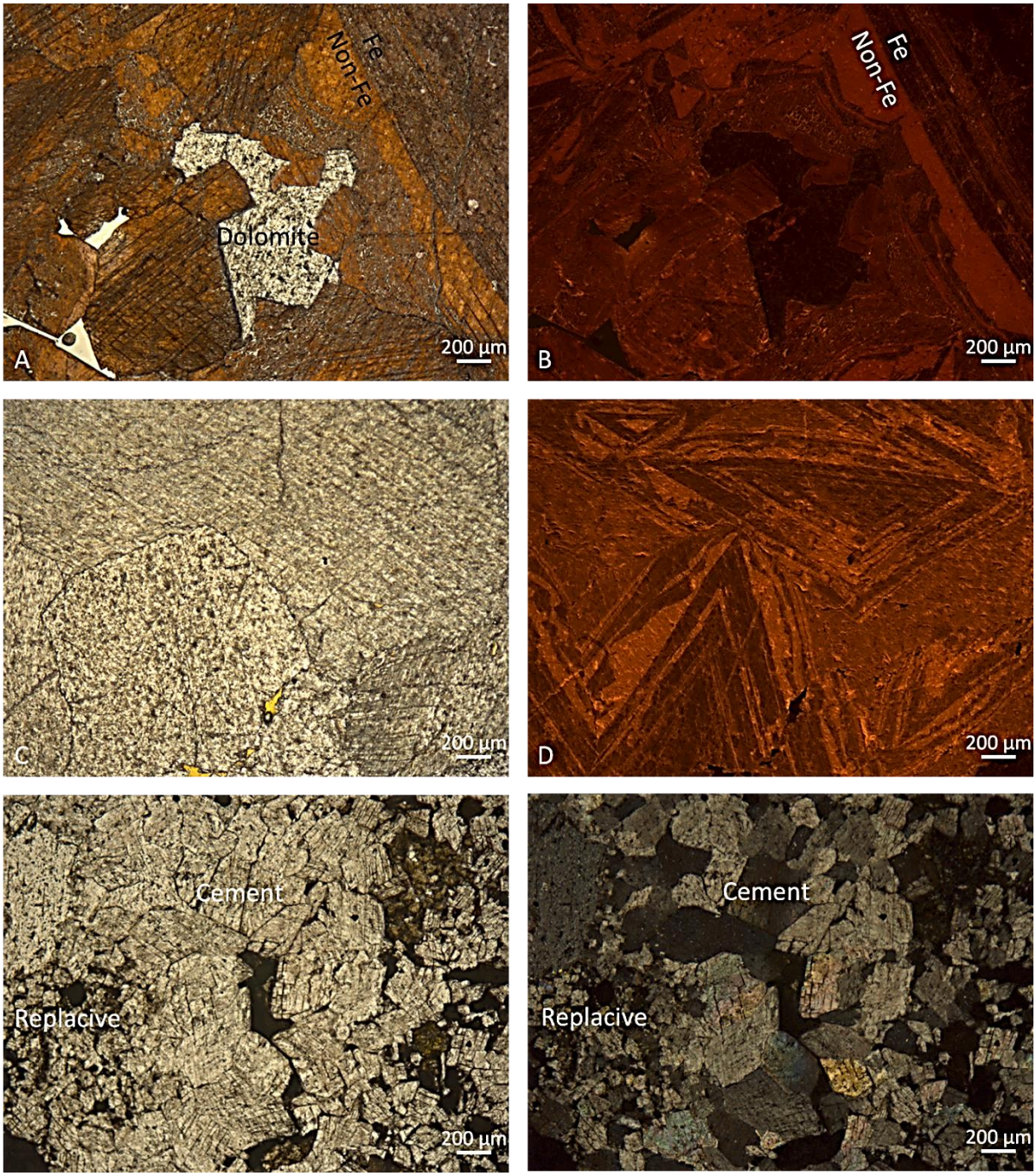

Figure 1-19: A – D) HYDROFRACTURES. E and F = MINERALISED KARST. A, B). Equivalent PPL and CL microphotograph. Staining for mineralogy of the thin section shows alternating zones of ferroan and non-ferroan calcite. The calcite predates non-luminescent dolomite (2379.10 m). Note the luminescence colours are attenuated due to the staining. C, D) The ferroan calcite is non-luminescent and the non-ferroan calcite is bright-dull luminescent (2379.10 m). E, F) Replacive dolomite consists of fine crystalline anhedral crystals. Coarser, saddle dolomite crystals occur in veins (2178.37 m).

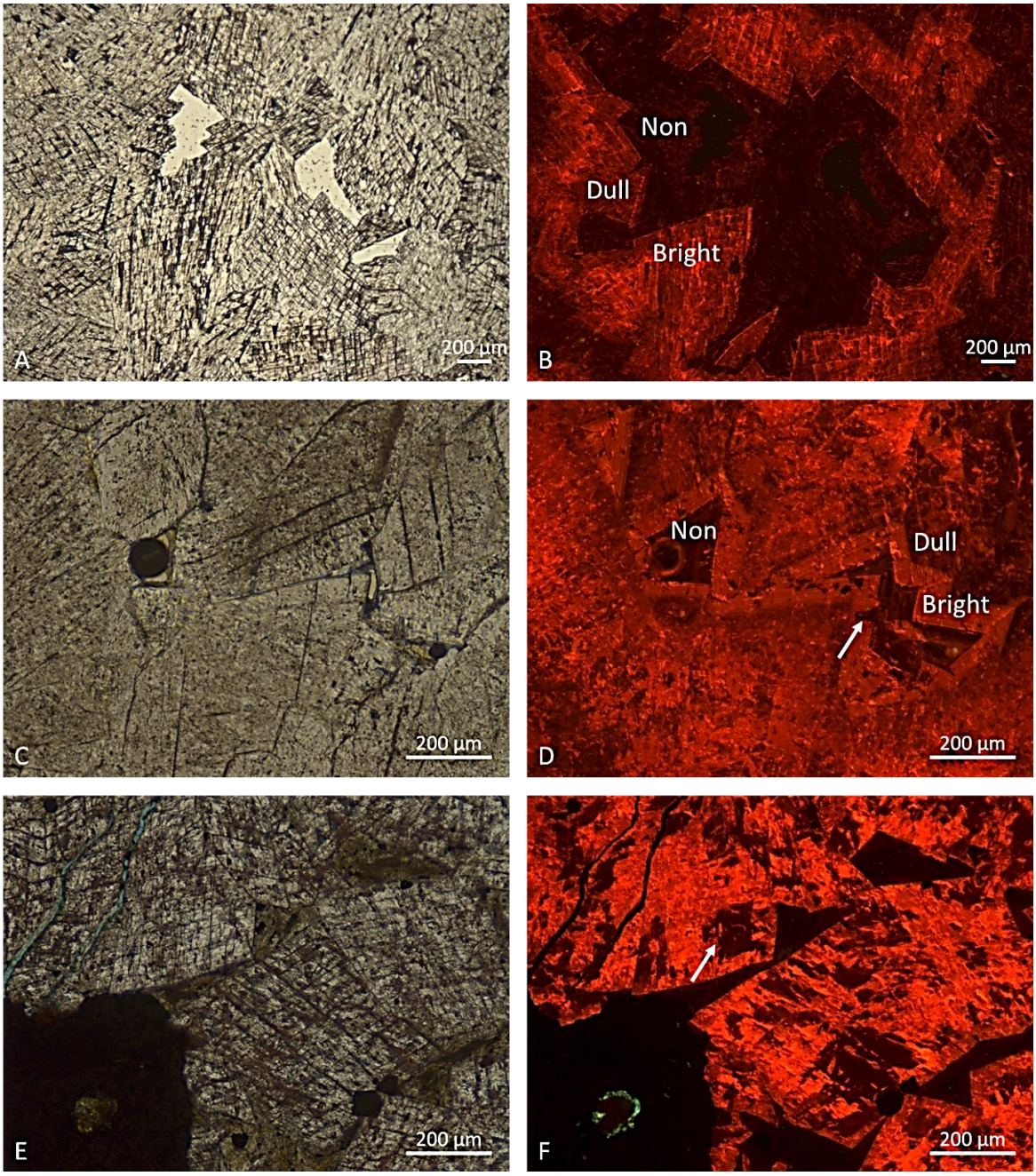

Figure 1-20: Mineralised karst. Equivalent PPL and CL microphotographs. A, B) Saddle dolomite crystals with bright, dull and non-luminescent zones (2178.37 m).C, D) The bright luminescent zones of saddle dolomite crystals are finely zoned. A phase of dissolution pre-dates the precipitation of the non-luminescent dolomite (white arrow) (2181.07 m). E, F) Recrystallisation of the saddle dolomite crystals is associated with the non-luminescent dolomite (white arrow) (2178.10 m).

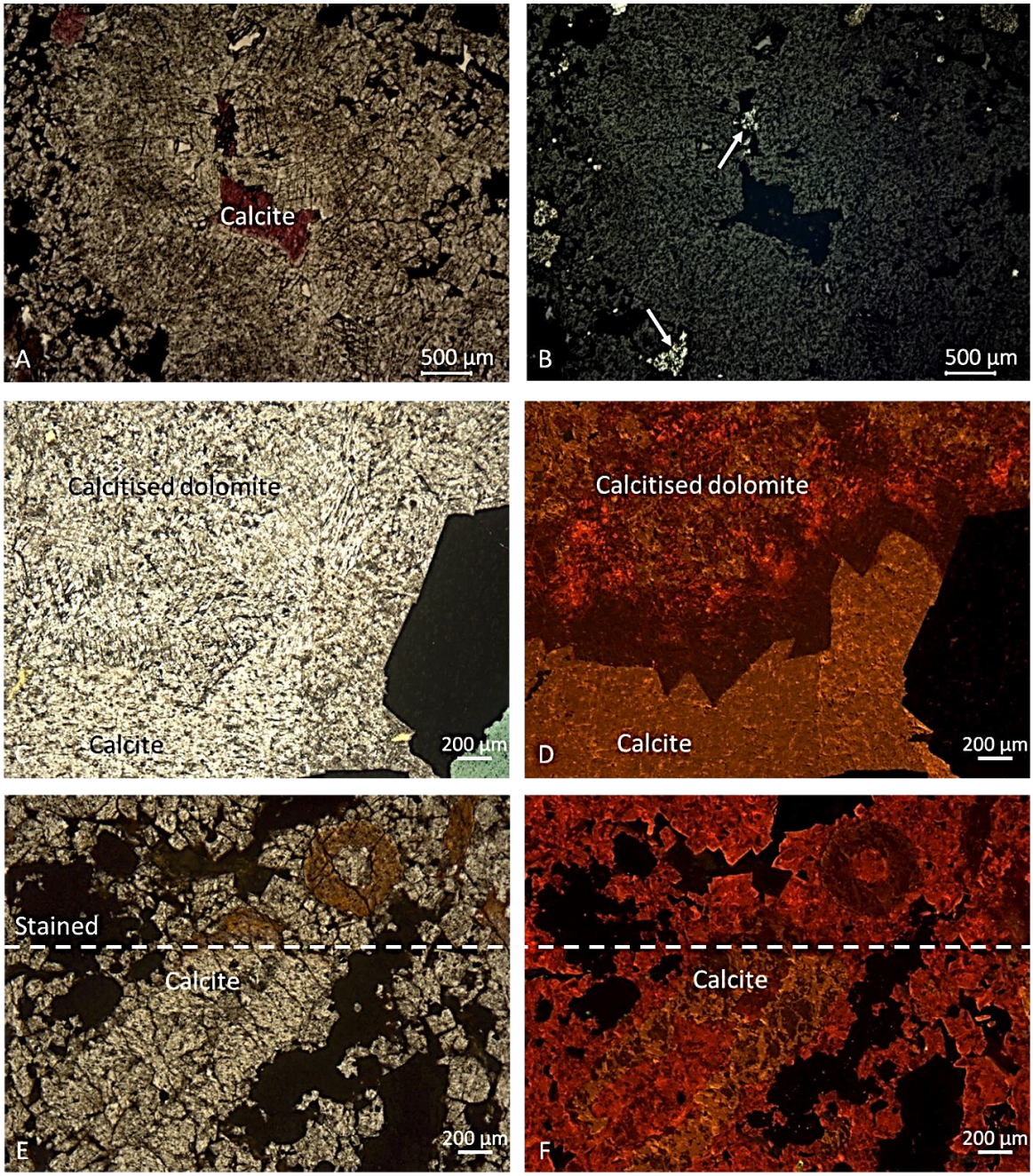

Figure 1-21: Mineralised karst. A, B) Equivalent PPL and reflected light microphotographs. Stained thin section. Calcite occludes intercrystalline pores of dolomite. Pyrite (white arrow) is associated with both dolomite and calcite (2178.37 m). C, D) The calcite postdating the dolomite is dull luminescent. Calcitisation/dedolomitisation of the dolomite can be observed as the luminescence zones of the dolomite are cross cut by the dull luminescent calcite (2181.28 m). E, F) Dull and bright luminescent calcite cementing moulds after crinoids (2178.37 m).

1.7.3 Stable isotopes

Nine samples were selected for stable isotope analysis (Table 1-5, Figure 1-22). The host rock/calcite matrix samples have depleted $\delta^{18}O$ values compared to the marine reference for Dinantian carbonates. The $\delta^{13}C$ values of host rock falls within the Dinantian marine reference range. The calcite phases cementing the hydrofractures have depleted $\delta^{18}O$ values similar to those of the host rock. Their $\delta^{13}C$ values are lower than those of the host rock. The stable isotope signature of the dolomite matrix signature is similar to that of the host rock. The dolomite veins are, however, characterised by more depleted $\delta^{18}O$ values.

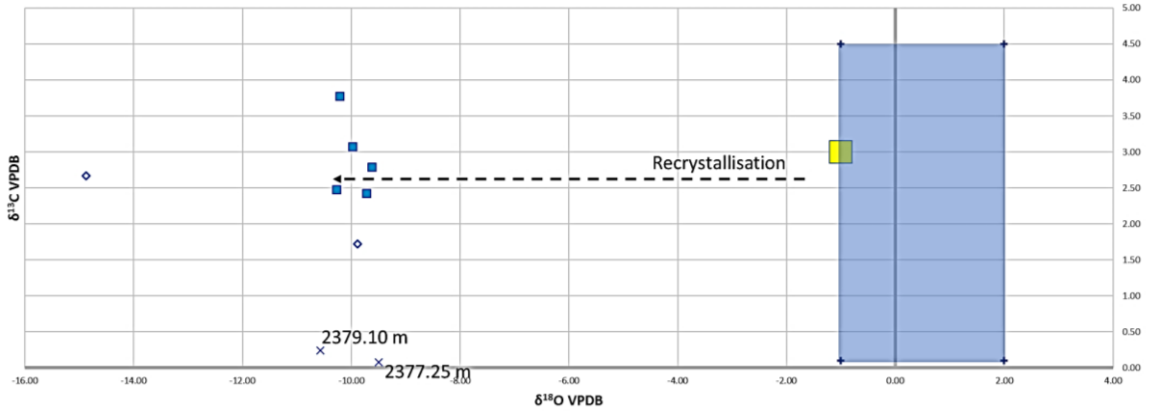

Figure 1-22: Stable isotope cross plot of the dolomite and calcite samples of the BHG-01, well. The blue filled symbols indicate the values for the matrix limestone; the blue diamonds indicate the values for the dolomite cements; the blue crosses show the values for calcite cements. The reference values of Dinantian marine limestones; yellow area after Muchez et al. (1991) and blue area after Nielsen et al. (1994).

Table 1-5: Overview of the results of the samples selected for stable O and C isotope analysis.

Sample (m)	Mineralogy	Diagenetic phase	matrix/vein	$\delta^{13}C$	$\delta^{18}O$
2379.1	Calcite	Cemented breccia	Matrix	3.08	-9.98
2181.07	Calcite	Carbonate clast in breccia	Matrix	2.43	-9.73
2381.7	Calcite	Limestone	Matrix	2.79	-9.63
2375.15	Calcite	Limestone	Matrix	3.77	-10.21
2377.25	Calcite	Limestone with calcite vein	Matrix	2.48	-10.28
2178.1	Dolomite	Fracture (dolomite) and sulphide mineralisation	Vein	2.67	-14.88
2379.1	Calcite	Hydrofracture cemented by Fe- and non-Fe calcite	Vein	0.24	-10.57
2181.07	Dolomite	Dolomitised breccia clast	matrix	1.72	-9.89
2377.25	Calcite	Hydrofracture cemented by calcite	Vein	0.08	-9.49

1.7.4 Fluid inclusion microthermometry

Two samples were selected for fluid inclusion microthermometry, i.e. 2178.37 m (karst) and 2379.10 m (hydrofractures).

The ferroan and non-ferroan calcite cementing hydrofractures (sample 2379.10 m) is characterised by temperatures ranging 78.4 °C < Th < 119.5 °C and 0.2-12.9 wt. % eq. NaCl (Table 1-6, Figure 1-23).

The dolomite (sample 2178.37 m) from the mineralised karst precipitation temperatures range between 77.4 and 120.4 °C (average 101.7 °C). The salinity of the fluid is highly variable, ranging between 1.4 and 8.3 wt. % eq. NaCl (Table 1-7, Figure 1-23).

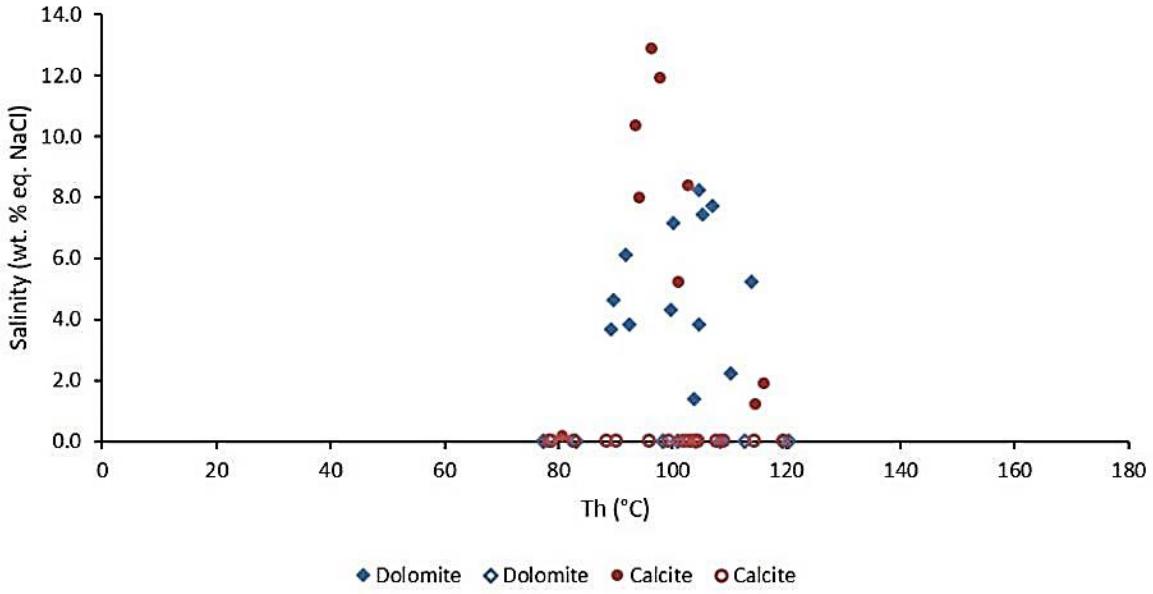

Figure 1-23: Temperature - salinity cross plot of the dolomite associated with pyrite mineralisation (BHG-01 2178.37 m) and calcite postdating the dolomite (2379.10 m). Metastable inclusions and inclusions for which Tm ice could not be observed have been attributed an arbitrary salinity of 0 wt. % eq. NaCl. These data points are marked by symbols without fill.

Table 1-6: Overview of the fluid inclusion microthermometry analysis of calcite samples obtained for BHG-01 2379.10 m. n.o. not observed.

F. i. Number	F. i. Type	F. i. Host mineral	F. i. Host type	$T_{m\,ice}$ (°C)	Salinity (wt. % NaCl eq)	T_h (°C)
1	aq	calcite	primary	n.o.		99.4
2	aq	calcite	primary	n.o.		104.0
3	aq	calcite	primary	n.o.		103.0
4	aq	calcite	primary	n.o.		90.2
5	aq	calcite	primary	-0.1	0.2	80.6
6	aq	calcite	primary	n.o.		82.7
7	aq	calcite	primary	met		78.9
8	aq	calcite	primary	n.o.		119.5
9	aq	calcite	primary	n.o.		114.4
10	aq	calcite	primary	n.o.		109.0
11	aq	calcite	primary	n.o.		107.8
12	aq	calcite	primary	n.o.		102.0
13	aq	calcite	primary	-1.1	1.9	116.1
14	aq	calcite	primary	-0.7	1.2	114.4
15	aq	calcite	primary	n.o.		78.4
16	aq	calcite	primary	n.o.		96.0
17	aq	calcite	primary	-5.1	8.0	94.1
18	aq	calcite	primary	-8.2	11.9	97.9
19	aq	calcite	primary	-9.0	12.9	96.3
20	aq	calcite	primary	n.o.		88.4
21	aq	calcite	primary	-5.4	8.4	102.8
22	aq	calcite	primary	-3.2	5.2	101.0
23	aq	calcite	primary	-6.9	10.4	93.6
24	aq	calcite	primary	n.o.		104.6

Table 1-7: Overview of the fluid inclusion microthermometry analysis of dolomite samples obtained for BHG-01 2178.37 m. n.o. not observed.

F. i. Number	F. i. Type	F. i. Host mineral	F. i. Host type	$T_{m\,ice}$ (°C)	Salinity (wt. % $NaCl_{eq}$)	T_h (°C)
1	aq	dolomite	primary	-1.3	2.2	110.2
2	aq	dolomite	primary	met		108.4
3	aq	dolomite	primary	-3.2	5.2	113.8
4	aq	dolomite	primary	n.o.		119.3
5	aq	dolomite	primary	n.o.		104.2
6	aq	dolomite	primary	-0.8	1.4	103.9
7	aq	dolomite	primary	-2.3	3.8	104.6
8	aq	dolomite	primary	-2.2	3.7	89.3
9	aq	dolomite	primary	met		98.4
10	aq	dolomite	primary	-2.8	4.6	89.6
11	aq	dolomite	primary	n.o.		100.8
12	aq	dolomite	primary	n.o.		112.7
13	aq	dolomite	primary	-4.7	7.4	105.3
14	aq	dolomite	primary	-4.9	7.7	107.0
15	aq	dolomite	primary	-4.5	7.1	100.2
16	aq	dolomite	primary	n.o.		77.4
17	aq	dolomite	primary	n.o.		83.1
18	aq	dolomite	primary	-2.3	3.8	92.5
19	aq	dolomite	primary	-3.8	6.1	91.7
20	aq	dolomite	primary	-2.6	4.3	99.7
21	aq	dolomite	primary	-5.3	8.3	104.6
22	aq	dolomite	primary	n.o.		120.4

1.7.5 Sulphur isotopes

Three analyses on the BHG-01 well were performed, two from the mineralised karst, and one from the dispersed pyrite in the limestone matrix (Table 1-2).

Table 1-8: Sulphur isotopes analyses performed in the well BHG-01.

Sample	δ^{34}S-CDT
BHG-01 2375.15 m	-29.14
BHG-01 2178.37 m	+15.10
BHG-01 2178.1 m	+17.83

The two values from the mineralised karst have similar Sulphur values (+15.10% and +17.83%) to the Carboniferous seawaters (Strauss, 2003) but they can also be interpreted as the marine evaporites, also shown for the St Ghislain well (south Belgium) to be $\delta\,^{34}S$ = +15.3 (Langguth and Nielsen, 1980). Similar values (+15.2%) was reported by Pierre and Rouchy (1986) for the Visean anhydrites deposits.

One sample (2375.15 m) coming from dispersed pyrite in limestone matrix, is very negative (- 29.14%). The negative values may indicate the sedimentary pyrite, but Nielsen et al. (2005) interpreted similar pyrites in Belgium as burial-related.

1.7.6 Diagenetic sequence in the context of burial/thermal history

D2 dolomites from the mineralised karst have average precipitation temperatures of 101.7°C, but have a variable salinity, with a near-meteoric component. Sulphur analysis suggest a marine origin for the sulphur in the associated pyrite. This would therefore suggest a mixed meteoric/burial origin to the fluids. It is known that the mineralisation postdates the Namurian-aged karst. But it is difficult to tie the mineralisation further. It is probable, however, that it represents a hydrothermal event. The calcites associated with hydrofracturing has similar fluid precipitation characteristics to the karst. There is some evidence for the hydrofracturing postdating mineralisation of karst (hydrofractures postdate dolomite). The hydrofractures are a product of overpressure release, and it is possible that this may be related to Cretaceous inversion or Paleogene tectonic activities. A precise timing of the mineralisation cannot be suggested due to the lack of appropriate samples and cross-cutting relationships. Based on Sr-Pb isotopic characteristics, Chatziliadou (2009) attributed the timing of mineralisation in the Stolberg-Aachen-Kelmis mining district (Germany) and Thermae 2002 (the SE Netherlands) to 134.3±1.3 and 134.5 ± 4.1 Ma, respectively, which defines a period of formation from the Late Jurassic to Early Cretaceous. More analogue data would be needed to confirm this.

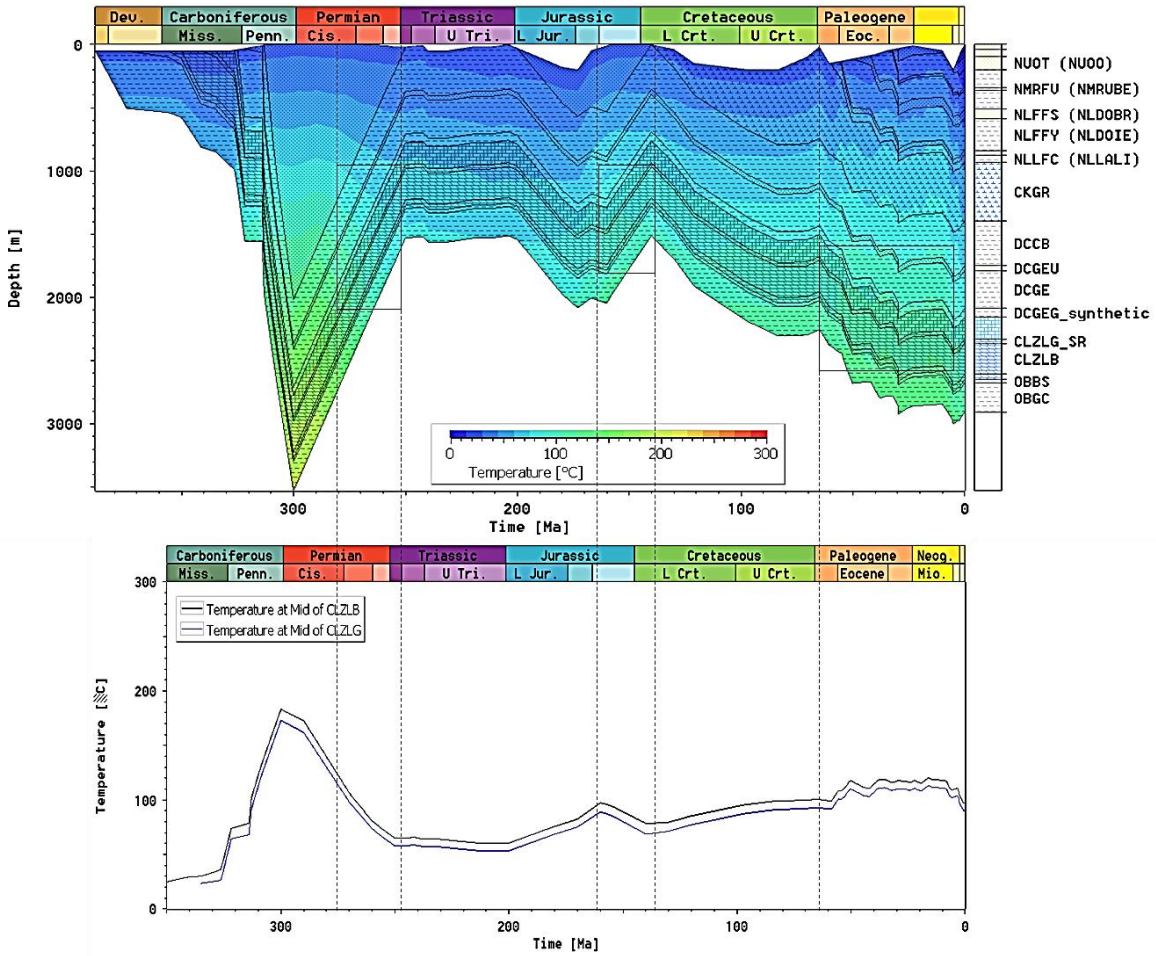

Figure 1-24: Temperature and burial histories tied to possible timing of the diagenetic events indicated by dashed lines and rectangles.

References

Langguth, H. R., & Nielsen, H. (1980). Sulphur isotopes in thermal waters and anhydrites of the Dinantian at the southern margin of the Brabant Massif: preliminary note. Mededelingen Rijks Geologische Dienst, 32(13), 101-105.

Muchez, P., Viaene, W.A., and Marshall, J. D. (1991a). Origin of shallow burial cements in the Late Visean of the Campine Basin, Belgium. Sedimentology Geology, 73, 257-271.

Nielsen, P., Swennen, R., and Keppens, E. (1994). Multiple-step recrystallization within massive ancient dolomite units: an example from the Dinantian of Belgium. Sedimentology, 41, 567-584.

Nielsen, P., Muchez, P., Heijlen, W., Tony Fallick, A. E., Keppens, E., Weis, D., and Swennen, R. (2005). Columnar calcites as testimony of diagenetic overprinting at the boundary between Upper Tournaisian dolomites and limestones (Belgium): multiple origins for apparently similar features. Sedimentology, 52(5), 945-967.

Pierre, C., and Rouchy, J. M. (1986). Oxygen and sulfur isotopes in anhydrites from Givetian and Visean evaporites of Northern France and Belgium. Chemical Geology: Isotope Geoscience section, 58(3), 245-252.

Staplin, F. L. (1977). Interpretation of thermal history from color of particulate organic matter-a review. Palynology, 1(1), 9-18.

Strauss, H. (2003). Sulphur isotopes and the early Archaean sulphur cycle. Precambrian Research, 126(3-4), 349-361.

Van Adrichem Boogaert, H. A. and Kouwe, W. F. P. (1994). Stratigraphic nomenclature of the Netherlands; revision and update by RGD and NOGEPA, Section B, Devonian and Dinantian, Mededelingen Rijks Geologische Dienst, 50 pp.

This page intentionally left blank

Daalsesingel 1
3511 SV Utrecht
scan@ebn.nl
www.scanaardwarmte.nl

Onderzoek in de ondergrond voor aardwarmte